European Journal of Mineralogy, 29(5): 915-922 (2017) DOI https://doi.org/10.1127/ejm/2017/0029-2630

Abellaite, $NaPb_2(CO_3)_2(OH)$, a new supergene mineral from the Eureka mine, Lleida province, Catalonia, Spain

Running title: Abellaite, a new basic Pb-Na carbonate mineral

Plan of the article: 1. Introduction, 2. Occurrence and general appearance, 3. Physical properties, 4. Powder X-ray diffraction, 5. Raman and FTIR spectroscopies, 6. Chemical data, 7. Discussion

Corresponding author: Jordi Ibáñez-Insa
Address: Institute of Earth Sciences Jaume Almera (CSIC)
Lluís Solé i Sabarís s/n, 08028 Barcelona, Catalonia, Spain
E-mail address: jibanez@ictja.csic.es
Phone number: +34 93 4095410

Abellaite, $NaPb_2(CO_3)_2(OH)$, a new supergene mineral from the Eureka mine, Lleida province, Catalonia, Spain

Jordi Ibáñez-Insa[1,*], José J. Elvira[1], Xavier Llovet[2], Jordi Pérez-Cano[1], Núria Oriols[3], Martí Busquets-Masó[1], Sergi Hernández[4]

[1] Institute of Earth Sciences Jaume Almera, ICTJA-CSIC, 08028 Barcelona, Catalonia, Spain
*Corresponding author, email: jibanez@ictja.csic.es
[2] Scientific and Technological Centres (CCiTUB), Universitat de Barcelona, 08028 Barcelona, Catalonia, Spain
[3] Museu Nacional d'Art de Catalunya (MNAC), Palau Nacional, Parc de Montjuïc, 08038 Barcelona, Catalonia, Spain
[4] Department of Electronics, Universitat de Barcelona, 08028 Barcelona, Catalonia, Spain

Abstract: The new mineral abellaite (IMA 2014-111), with ideal formula $NaPb_2(CO_3)_2(OH)$, is a supergene mineral that was found in one of the galleries of the long-disused Eureka mine, in the Southern Pyrenees (Lleida province), Catalonia, Spain. Abellaite is found as sparse coatings on the surface of the primary mineralization, and forms subhedral microcrystals not larger than 10 μm as well as larger pseudohexagonal crystals up to ~30 μm. Individual microcrystals usually have a tabular habit and form fairly disordered aggregates. The mineral is associated with a large number of primary minerals (roscoelite, pyrite, uraninite, coffinite, carbon, galena, sphalerite, nickeloan cobaltite, covellite, tennantite, chalcopyrite) and supergene minerals (hidrozincite, aragonite, gordaite, As-rich vanadinite, andersonite, čejkaite, malachite, devilline). Abellaite is colourless to white, with a vitreous to nacreous lustre. The mineral is translucent, has a white streak, and is non-fluorescent. The aggregates of microcrystals are highly friable. The calculated density using the ideal formula is 5.93 g/cm^3. The chemical composition of the mineral (the mean of 10 electron microprobe analyses) is: Na 3.88, Ca 0.29, Pb 72.03, C 4.17, O 19.47, H 0.17, total 100.00 wt%, obtained with matrix correction calculations. H, C and O have been determined by stoichiometry assuming the ideal formula. On the basis of 7 O atoms, the empirical formula of abellaite is $Na_{0.96}Ca_{0.04}Pb_{1.98}(CO_3)_2(OH)$. The simplified formula of the mineral is $NaPb_2(CO_3)_2(OH)$. The mineral is hexagonal, space group $P6_3mc$, a = 5.254(2), c = 13.450(5) Å, V = 321.5(2) Å^3, Z = 2. The strongest powder-diffraction lines [d in Å (I) (hkl)] are: 3.193 (100) (013), 2.627 (84) (110), 2.275 (29) (020), 2.242 (65) (021,006), 2.029(95) (023). Abellaite has a known synthetic analogue, and the crystal structure of the mineral was refined by using crystallographic data of the synthetic phase. The mineral is named in honour of the mineralogist and gemmologist Joan Abella i Creus (b. 1968), who has longed studied the minerals of the Eureka mine and who collected the mineral.

Key-words: abellaite; basic carbonate; lead carbonate; secondary mineral; supergene mineral; uranium mine; Eureka mine, Catalonia, Spain

1. Introduction

The Eureka mine, located in the Catalan Pyrenees (Lleida province), is an abandoned U mine that provides a useful reference example of Cu-U-V ore mineralizations and their supergene evolution. Today, the Eureka mine is well-known among researchers and amateur collectors for the numerous minerals it features, both from stratabound mineralizations and from the supergene alteration of the ores. Exotic species such as čejkaite, demesmaekerite, metamunirite, or natrozippeite have been reported from this long-disused mine (Abella & Viñals, 2009; Abella & Viñals, 2012; Castillo *et al.*, 2009). So far, however, no new mineral species had been found in this location.

Abellaite is a new basic Pb-Na carbonate mineral found in one of the galleries of the Eureka mine, further demonstrating the abundance of unusual rare species in this site. The mineral was named in honour of the amateur mineralogist and mineral collector Joan Abella i Creus (b. 1968) from Sabadell, Catalonia, Spain, who collected the mineral and who has long contributed to the mineralogical study of different deposits in Catalonia, including the Eureka mine. The mineral and its name have been approved by the International Mineralogical Association Commission of New Minerals, Nomenclature and Classification (IMA no. 2014-111).

Abellaite has a known synthetic analogue (Brooker *et al.*, 1982; Krivovichev & Burns, 2000; Belokoneva *et al.*, 2002), which was investigated due to potential applications of lead carbonates in nuclear-waste management and non-linear optics. Co-type material is deposited in the collections of the Natural History Museum of Barcelona, Catalonia, Spain, catalogue number MGB 26.350.

2. Occurrence and general appearance

The Eureka mine (42° 23' 10" N, 0° 57' 27" E) is an abandoned U mine that was subject to a mining exploration project during the 50's and 60's of the last century. It is located in the Vall Fosca (Lleida Province), Southern Pyrenees, adjacent to the Flamisell river and very close to the small village of Castell-estaó, which belongs to the municipality of la Torre de Capdella in the Pallars Jussà, Catalonia, Spain. Here we spell Capdella (the locally preferred spelling) instead of Cabdella, the official denomination.

The Eureka mine is located in a complex geological area (see Fig. 1), affected by huge tectonic activity during the end of the Paleozoic era and by the development of the Pyrenees between the Late Cretaceous and Oligocene as a consequence of the inversion of rift basins (Vergés & Muñoz, 1990; Muñoz *et al*., 1992). Owing to the latter, Palaeozoic and Mesozoic materials are displaced by several thrust sheets. The continental record of Carboniferous and Permian periods is discordant with marine organic-rich Devonian sediments, exhibiting intrabasinal discontinuities and volcanic levels. The contact between Permotriassic materials (Buntsandstein facies) shows an erosive discordance with the Lower and Middle Permian sequences, whereas the rest of Triassic (Muschelkalk and Keuper), Jurassic and Cretaceous sediments are paraconcordant (Mey *et al.*, 1968). At the top of the Triassic sediments, small outcrops of late-Triassic ophites can be found, probably related to the Atlantic opening (Béziat *et al.*, 1991). On top of these units, the continental post-tectonic Tertiary conglomerates mark the end of the Pyrenean uplift.

The Eureka mine features four distinct stages of mineralization originated at different geological times: (i) the primary (stratabound) U-V-Cu mineralizations, (ii) ore mineralizations due to tectonic activity during the Eocene and Oligocene, (iii) natural supergene enrichment by chemical weathering and redeposition of dissolved species through the oxidized zone down to the enriched zone, and (iv) neoformation of secondary minerals by chemical weathering and redeposition due to post-mining supergene processes on mine walls.

The primary U-V-Cu mineralizations are hosted within the fluvial continental Buntsandstein redbeds, and are composed of millimetre-sized grains of different minerals containing Cu-V-U-Bi-Ag-Se-As-Ni-Co, such as sulphides, sulfosalts, selenides, U-V oxides, silicates or native elements minerals (Castillo *et al.*, 2009). The Kupferschiefer deposit (German-Poland) or the uranium deposits at Karoo Basin (South Africa) are similar cases of valuable U-V-Cu deposits associated with redbed sequences and which have been mined for the extraction of these elements (Turner, 1985). The lower panel of Fig. 1 shows the redbed sediments next to the gallery entrance where abellaite was found. Just to the right side of the gallery, the sediments exhibit the characteristic red-brown colour due to the presence of ferric oxides (note that the strata are almost vertical due to tectonic activity). As can be seen in the picture, on top of the gallery entrance the sediments exhibit the typical greyish colour corresponding to a

105 reduced zone, i.e., where U-V-Cu stratabound mineralizations in redbeds mainly occur.
106 In this case, the mineralizations were probably favoured by the underlying presence of
107 organic matter arising from the Devonian limestones, just below the Buntsandtein
108 redbeds (see Fig. 1).

109 The second stage of mineralization in the Eureka mine is related to the end of the
110 Pyrenean orogeny (Eocene-Oligocene). In this case, tectonic efforts due to Alpine
111 deformation gave rise to remobilization of the chemical species, filling small veins,
112 faults and joints with minerals such as quartz, ankerite and some sulphur minerals
113 (Castillo *et al.*, 2009). The two final stages of mineralization are related to supergene
114 processes. On the one hand, natural pseudomorphic replacements of the primary ores
115 gave rise to a large number of secondary oxidized minerals including sulphates,
116 arseniates, phosphates, vanadates or seleniates, many of which contain U (Castillo *et al.*,
117 2009). On the other hand, numerous neoformation, post-mining minerals are deposited
118 on the walls of the mine, occurring as encrustations, coatings or cryptocrystalline
119 efflorescences.

120 Abellaite, similarly to other carbonates such as andersonite or čejkaite found in the
121 Eureka mine, belongs to this latter group of post-mining secondary minerals originated
122 by supergene enrichment. The mineral forms sparse coatings on the surface of the
123 primary mineralization (see Fig. 2a), most often on a substrate of quartzite, with
124 primary-ore minerals such as roscoelite, pyrite, uraninite, coffinite, carbon, galena,
125 sphalerite, native bismuth, Ni-rich cobaltite, covellite, tennantite, or chalcopyrite.
126 Quartz from the detrital sediments and roscoelite are very common in all the samples
127 investigated.

128 The typical coverage of the specimens is of about 1 to 10 mm^2, although somewhat
129 larger clusters of about 1 cm^2 have also been observed. In general, the mineral forms
130 subhedral microcrystals not larger than 10 μm, as shown in Fig. 2b. However, some
131 larger (from 10 up to 30 μm) idiomorphic, pseudohexagonal crystals with a prominent
132 pinacoid face (and more poorly developed prism faces) are also observed (Figs. 2c and
133 2d). Pyramid-like forms are barely observed. As can be seen in Fig. 2d, the more
134 euhedral microcrystals have a tabular habit and form fairly disordered aggregates. The
135 mineral may also found to exhibit a crown-like texture when it coats pre-existing
136 minerals with globular habit.

In addition to the primary ore minerals mentioned above, the individual specimens investigated contain many of the supergene minerals that have been reported from the Eureka mine (Castillo *et al.*, 2009). These include andersonite, calcium carbonate (probably aragonite), gordaite, andersonite, čejkaite, malachite, natrozippeite or devilline. Other unreported supergene minerals such as hydrozincite or As-rich vanadinite have also been found in close association to abellaite (see Fig 3).

3. Physical properties

The aggregates of abellaite are colourless to white, with a vitreous to nacreous lustre. The mineral is translucent and has a white streak. No fluorescence was observed under short-wave (254 nm) and long-wave (366 nm) ultraviolet (UV) illumination. Chemical tests indicated that abellaite is not soluble in water, but seems to incongruently dissolve in 20% HCl at room temperature, with separation of $PbCl_2$. Due to the small size of the microcrystals and the difficulty to separate the mineral from the substrate, cleavage and fracture are not observable for individual microcrystals. In the synthetic analogue, the crystals were found to exhibit perfect cleavage along the (001)-plane (Belokoneva *et al.*, 2002).

Similarly, owing to the small size of the microcrystals, the hardness and density of the mineral cannot be measured. The aggregates of microcrystals in the as-collected specimens are relatively soft, with marked friability. The calculated density of the mineral, using the empirical formula and X-ray powder diffraction data, is 5.90 g/cm^3. This value is very similar to that obtained with the ideal formula (5.93 g/cm^3).

On account of the structural properties and crystal structure of abellaite (see below), the mineral is probably uniaxial. However, it cannot be ruled out that the mineral may exhibit anomalous biaxiality due to lattice strains induced by chemical substitutions or defects (Foord & Mills, 1978). A tentative determination of the refractive index of the mineral, using available immersion liquids and by comparison to grains of other minerals like cerussite or corundum, suggested that the average refractive index of the mineral should be below 2 and somewhat larger than 1.8. This observation is in excellent agreement with the value extracted from the Gladstone-Dale relationship, which predicts an average refractive value for abellaite of 1.90. However, given that the available material is polycrystalline, and given that single-crystal fragments are so small and friable (note also that they are adhered to the substrate and associated minerals, see

next section), the result obtained with the immersion liquids is probably somewhat fortuitous. For these same reasons, it was not possible to determine optic sign, birefringence, or dispersion of the mineral. No pleochroism was observed under the microscope.

4. Powder X-ray diffraction

Four different types of powder X-ray diffraction (XRD) measurements were performed on the mineral: i) Micro-diffraction measurements on hand-picked grains with a PANalytical X'Pert PRO MPD powder diffractometer (CuKα_1 radiation, λ = 1.5406 Å) at the Scientific and Technical Centres of the University of Barcelona, equipped with a linear position-sensitive (PSD) Si strip X'Celerator detector and a primary Ge(111) Johansson-type monochromator; ii) Conventional Bragg-Brentano measurements on large (and as flat as possible) areas of as-collected abellaite aggregates, using a Bruker D5005 powder diffractometer (CuKα_1 radiation, λ = 1.5406 Å) at ICTJA-CSIC, equipped with a scintillator detector and a secondary Ge(111) monochromator; iii) XRD measurements on a few tens of hand-picked grains with a Bruker D8-A25 diffractometer (CuKα_1 radiation, λ = 1.5406 Å) at ICTJA-CSIC, equipped with TWIN-TWIN optics and a linear PSD Lynxeye detector, and configured in Bragg-Brentano mode of operation, using a Si single-crystal low-background sample holder and long integration times; iv) XRD measurements on small (~1 mm^2) areas of as-collected dense abellaite aggregates, with the same Bruker D8-A25 powder diffractometer (CuKα_1 radiation, λ = 1.5406 Å) at ICTJA-CSIC, using a Göbel mirror and a 300-µm collimator in the primary optics to reduce the area of analysis.

The first micro-diffraction measurements on hand-picked grains (i) allowed us to detect numerous reflections from different phases, including quartz and roscoelite. However, the identification (or indexing) of the unassigned peaks was not possible. We thus concluded that single-crystal XRD studies of abellaite could not be carried out, since the mineral is too-fine grained and cannot be separated from the substrate and associated minerals.

Instead, and in spite of the large broadening expected for the conventional Bragg-Brentano geometry (ii) due to sample roughness, these measurements turned out to be

crucial to identify the mineral. For these measurements, relatively flat areas of the samples were selected to reduce the width of the XRD peaks. Figure S1, which is freely available online as Supplementary Material linked to this article on the GSW website of the journal, http://eurjmin.geoscienceworld.org, shows a diffraction scan of abellaite, together with the diffraction pattern of synthetic $NaPb_2(CO_3)_2(OH)$ from Brooker *et al.* (1982), where this phase was indexed as hexagonal. As can be seen in the figure, the pattern of the synthetic phase closely matches the XRD scan. Thus, given the chemical data and the results of vibrational spectroscopies (Raman and IR, see below), these XRD measurements indicate that the mineral is the natural analogue of synthetic $NaPb_2(CO_3)_2(OH)$.

We would like to mention that, after these results, we were able to identify several reflections from the $NaPb_2(CO_3)_2(OH)$ phase in the micro-diffraction scans obtained from hand-picked material (i). In the case of the XRD scans obtained from several hand-picked grains by using a low-background sample holder (iii), the XRD peaks from abellaite are more easily identified, as can be seen in Fig. S2. In such case, and most likely because more amount of the mineral is measured, the peaks from $NaPb_2(CO_3)_2(OH)$ clearly show up in the scans, which further confirms that abellaite is the natural analogue of this synthetic compound. In these scans, however, the (00*l*) reflections from roscoelite are also visible, which indicates that these measurements are strongly affected by preferential orientation of the grains.

The powder XRD measurements obtained with conventional Bragg-Brentano measurements (ii) and those obtained from millimeter-sized areas of dense aggregates of abellaite (iv) allowed us to refine the cell parameters and atomic positions of the mineral. Rietveld refinements were performed with the program TOPAS 4.2, from Bruker. In some cases, weak peaks from associated minerals such as quartz or roscoelite showed up in the scans. These additional features were taken into account in the refinements by including additional peaks. As starting point, here we employ the structural information of $NaPb_2(CO_3)_2(OH)$, space group $P6_3mc$, from Krivovichev & Burns (2000a). We would like to note that Belokoneva *et al.* (2002) synthesized $NaPb_2(CO_3)_2(OH)$ crystals and inferred a $P31c$ space group from the analysis of systematic absences in single-crystal XRD measurements. In the present work we have relied on the data from Krivovichev & Burns (2000a) because application of the

Addsym tool from the Platon program (Spek, 2009) indicates that the *P*31*c* structure has missing symmetries, which does not occur in the case of the $P6_3mc$ structure.

Table 1 shows the powder diffraction data thus obtained. Note that at low (measured) lattice spacings, d_{meas}, the observed XRD peaks are fairly broad and weak, and therefore numerous reflections contribute to those features. Thus, below 1.75 Å the d_{meas} values given in Table 1 correspond to the observed peak maxima.

The hexagonal unit-cell parameters refined from the powder data are: a = 5.254(2), c = 13.450(5) Å and V = 321.5(2) Å^3. These values are close to those reported by Brooker *et al.* (1982) (a = 5.273(2), c = 13.448(5) Å), Krivovichev & Burns (2000a) (a = 5.276(1), c = 13.474(4) Å) and also to those of Belokoneva *et al.* (2002) (a = 5.268(4), c = 13.48(1) Å). Crystallographic information of abellaite is shown in Table 2. The resulting atomic positions of the mineral, starting from the structural information in Krivovichev & Burns (2000a), are given in Table 3. The values thus obtained are not far from those obtained in that work. The thermal parameters were not refined in the present study, since the errors in these parameters were too large. Thus, the isotropic thermal displacement parameters given in Table 3 are the same as in Krivovichev & Burns (2000a).

5. Raman and FTIR spectroscopies

Raman spectra were excited with the second harmonic of a continuous-wave Nd:YAG laser (λ = 532 nm). The spectra were acquired with a Horiba Jobin-Yvon LabRam spectrometer coupled to a high-sensitive CCD detector, using a long-working distance 50x objective that produced a ~4 μm laser spot on the sample. A notch-filter was employed to filter out the elastically scattered (Rayleigh) radiation, providing access to Raman signals above ~100 cm^{-1}. The spectra were directly obtained from denser aggregates of abellaite microcrystals on as-collected specimens.

A typical Raman spectrum of abellaite is shown in Fig. 4a. As can be seen in the figure, the spectra are dominated by a sharp band at ~1058 cm^{-1} and a weaker, broader feature at ~1391 cm^{-1} that can be attributed to symmetric (υ_1) and asymmetric (υ_3) stretching modes of CO_3^{2-} groups, respectively (Brooker *et al.*, 1983). As in most carbonate compounds, the υ_1 peak is the strongest feature in the Raman spectra. In the high-wavenumber region (~3504 cm^{-1}), a weak peak arising from O-H stretching vibrations

shows up in the spectra, confirming the presence of hydroxyl groups in the crystal structure of abellaite. These two observations support the XRD results, i.e., the assignment of the mineral to a basic carbonate compound. Frequency values for the different spectral features that appear in Fig. 4a are listed in Table 4. For comparison, the Table also shows the Raman features above 200 cm^{-1} reported in Brooker *et al.* (1983) for the case of synthetic $NaPb_2(CO_3)_2(OH)$. As can be seen by comparing the data from both works, the Raman spectrum of abellaite closely resembles that of the synthetic $NaPb_2(CO_3)_2(OH)$ samples studied in Brooker *et al.*(1983). It should be noted, however, that a few additional weak features appear in the spectra of abellaite. Most likely, these bands arise from associated minerals, as is the case of the weak, sharp peak at ~465 cm^{-1}, which we assign to quartz. However, it cannot be ruled out that some of these peaks actually correspond to abellaite. From one hand, it should be recalled that $NaPb_2(CO_3)_2(OH)$ has 26 atoms in the unit cell and therefore 78 normal modes of vibration, 32 of which correspond to Raman-active optical modes [$\Gamma_{opt}=9A_1 + 11E_1 + 12E_2$, as follows from group-theory analysis of the vibrational modes of $NaPb_2(CO_3)_2(OH)$, space group $P6_3mc$, as in Krivovichev & Burns (2000a)]. Thus, given that abellaite is found as aggregates of small microcrystals (while Brooker *et al.*, 1983 studied synthetic samples containing much larger crystals), some of the observed peaks might correspond to Raman-active modes of abellaite that would not be observed in single-crystalline material. On the other hand, lattice distortions or incorporation of impurities in the lattice of abellaite could also give rise to these additional modes.

The close resemblance between the vibrational properties of abellaite and synthetic $NaPb_2(CO_3)_2(OH)$ is further supported by means of Fourier transformed infrared (FTIR) spectroscopy measurements, which were obtained by using a Spotlight 150 microscope interfaced to a Frontier (Perkin Elmer) spectrometer. For this purpose, hand-picked material in form of microcrystalline aggregates of the mineral was loaded into a diamond anvil cell. FTIR transmission analyses were acquired with 4 cm^{-1} resolution by integrating 32-64 scans from 550 to 4000 cm^{-1}. Figure 4b shows a FTIR spectra of abellaite, which is dominated by the characteristic, strong band at ~1425 cm^{-1} arising from the υ_3 asymmetric internal stretching modes of the CO_3^{2-} group. Weaker bands that can be assigned to the out-of-plane and in-plane bending modes (υ_2, υ_4) and to the υ_1-symmetric stretching modes of CO_3^{2-} also appear in the spectra (see Table 5). In addition to these fundamental modes, the spectra also show the characteristic absorption

bands of OH-stretching at ~3500 cm^{-1}. The band at ~998 cm^{-1} can also be tentatively assigned to PbOH bending vibrations (Brooker *et al*., 1983). The observation of characteristic absorption bands of CO_3^{2-} and OH^- groups confirms that the mineral is a basic carbonate compound. Table 5 gives measured frequencies in our sample and data from Brooker *et al.* (1983) and Belokoneva *et al.* (2002). As in the case of the Raman results, the IR spectra are very similar to those of synthetic $NaPb_2(CO_3)_2(OH)$ (Brooker *et al.*, 1983; Belokoneva *et al.*, 2002). Again, however, it should be noted that some minor differences are observed between the three works (and also between Brooker *et al.* (1983) and Belokoneva *et al.* (2002), see Table III). As in the case of the Raman data, the observed differences can be mainly attributed to the origin of the investigated samples (natural vs synthetic) and also to the presence of accessory minerals and impurities in the case of the natural specimens. The present FTIR measurements, however, confirm that abellaite is a basic carbonate compound, very similar to the synthetic phases studied in previous works.

6. Chemical data

Chemical analyses of abellaite crystals were carried out using a JEOL JXA-8230 electron microprobe at the Scientific and Technological Centres of the University of Barcelona. The samples were set in epoxy resin and subsequently polished. The mount thus obtained allowed us to identify around 10 microcrystals of abellaite for chemical analysis. Figure 3 displays backscattered electron (BSE) micrographs showing some of the analysed crystals, with sizes ranging from 2 μm to 10 μm. Wavelength-dispersive spectrometry (WDS) measurements were conducted using a 10 kV accelerating voltage and 2 nA beam current with a defocused 2 to 5 μm spot in order to both minimize surface damage of the crystals (Iizuka *et al.,* 2012) and improve the spatial resolution of the analyses. For this material, the penetration range of the incident electrons drops from 2.75 μm at 20 kV accelerating voltage down to 0.85 μm at 10 kV accelerating voltage (estimation performed using the auxiliary program "Tables" from the PENELOPE distribution (Salvat, 2015)). Counting times were 30 s peak and 15 s background for all analysed elements (Ca, K, Na and Pb). In order to improve counting statistics, Na and Pb were simultaneously measured with two spectrometers, using TAP and TAPH crystals for Na, and PETH and PETL crystals for Pb. No other elements were detected with the WDS scans. Standards used for calibration were: caracolite $[Na_3Pb_2(SO_4)_3Cl]$ for Na, cerussite for Pb, orthoclase for K and calcite for Ca. The

matrix correction procedure XPP (Pouchou and Pichoir, 1988) was used to convert specimen intensity ratios into concentrations. The matrix correction calculations were carried out by means of O stoichiometry (Lane & Dalton, 1994), considering CO_2 by difference to 100%. C-H-N elemental analyses were not performed because it was not possible to unambiguously isolate the hand-picked mineral from the substrate and accessory minerals, as found by XRD measurements. Thus, O, C and H were determined by stoichiometry assuming the ideal formula of the synthetic compound. The average of 10 electron-microprobe determinations and the corresponding ranges are given in Table 6. On the basis of 7 O atoms, the resulting charged-balanced empirical formula for the mineral is $Na_{0.96}Ca_{0.04}Pb_{1.98}(CO_3)_2(OH)$, while the ideal formula is that of the synthetic phase [$NaPb_2(CO_3)_2(OH)$].

7. Discussion

On the basis of X-ray powder diffraction data, vibrational spectra (Raman and IR) and chemical composition, it can be concluded that abellaite is closely related to the synthetic compound $NaPb_2(CO_3)_2(OH)$ studied by several authors (Brooker *et al.*, 1982; Krivovichev & Burns, 2000; Belokoneva *et al.*, 2002). The fact that the same conclusion is reached with techniques based on different principles (i.e., vibrational vs structural) indicates that the chemical formula of the mineral must be very close to that of the synthetic phases. Although a direct determination of H_2O and CO_2 contents was not possible due to the small size of the microcrystals, the WDS measurements did confirm that the Pb/Na ratio of the mineral is close to 2 as in the synthetic phase. As suggested by the WDS data, however, abellaite may also contain Ca ions, which are probably incorporated into Pb sites because these two elements may have the same valence (2+). However, taking into account the close ionic radii of Na and Ca, it cannot be ruled out that Ca may also substitute for Na in the mineral.

Abellaite adds to the list of uncommon carbonate minerals found in the galleries of the Eureka mine, such as andersonite, čejkaite, bayleyite, liebigite, or schröckingerite (Abella i Creus & Viñals, 2009; Abella i Creus & Viñals, 2012). Following the results of Krivovichev & Burns (2000a), the mineral crystallizes in the hexagonal system, space group $P6_3mc$. As discussed by these authors, this phase contains a hexagonal sublattice of Pb atoms and therefore the structure can be related to the structure of other Pb hydroxide carbonates such as plumbonacrite (see also Krivovichev & Burns, 2000b).

The crystal structure of abellaite is also closely related to that of the recently approved new mineral grootfonteinite $Pb_3O(CO_3)_2$ (Siidra *et al.*, 2015). This mineral crystallizes in the space group $P6_3mc$ with lattice parameters a = 5.303(1) Å and c = 13.770(2) Å, which are only slightly larger than those of abellaite.

According to its chemical composition, abellaite is closely related to hydrocerussite, plumbonacrite, and sanrománite. In the New Dana classification, abellaite can be assigned to the carbonates, hydroxyl class (16a) and, similarly to hydrocerussite (trigonal, space group R-3m), to the group of carbonates - hydroxyl or halogen, $(AB)_3(XO_3)_2Zq$ (subgroup 16a.02). In the Nickel-Strunz classification, as in the case of hydrocerussite, the mineral can be classified as a carbonate with additional ions, without H_2O, with Pb or Bi (subgroup 5.BE). Both plumbonacrite and sanrománite crystallize in the hexagonal system, $P6_3mc$. Sanrománite is an anhydrous carbonate that also incorporates Ca cations, which further suggests that other (basic, hydrated or anhydrous) carbonates with Pb, Ca, Na and also K may also be found in nature.

With regard to this, we would like to mention that a recent analysis on carbon mineral ecology applying a Large Number of Rare Events (LNRE) model has predicted that numerous (~145) undiscovered carbon mineral species may exist on Earth (Hazen *et al.*, 2016). According to these predictions, a large subset of such undescribed minerals should be compounds of O, H, Ca, and Na. This is the case of $NaPb_2(CO_3)_2(OH)$, which is listed in Hazen *et al.* (2016) as one of the possible missing carbon minerals. According to the LNRE predictions, other basic or hydrated carbonate minerals, compatible with the oxidizing conditions of secondary mineralizations like those involved in the formation of abellaite, could also be found. More work is thus required to identify and describe possible new carbon minerals and to confirm the predictions of that work.

Acknowledgements: This paper is dedicated to the memory of our colleague and friend Prof. Joan Viñals, who passed away on November 2013. Professor Viñals was an expert mineralogist who studied different new species such as barahonite and who initiated the characterization of abellaite. We are grateful to Joan Abella i Creus for supplying us with the mineral samples and for useful information about the mineral and the Eureka mine. We would like to thank Eva Perisé and the Town Hall of Torre de Capdella for

392 valuable support and assistance. Work partially funded by ERDF-EU Ref. CSIC10-4E-
393 141.

References

Abella i Creus, J. & Viñals, J. (2009): Čejkaite, arsenuranylite, compreignacite, natrozippeite and other rare uranium minerals in the Eureka mine, Castell-estaó, La Torre de Cabdella, Lleida, Catalonia. *Mineral Up*, **2**, 52–71.

Abella i Creus, J. & Viñals, J. (2012): New minerals from the Eureka mine: metamunirite, schröckingerite, boltwoodite and gordaite, Castell-estaó, la Torre de Cabdella, Lleida, Catalonia, Spain. *Mineral Up*, **3**, 14–18.

Belokoneva, E.L., Al'-Ama, A.G., Dimitrova, O.V., Kurazhkovskaya, V S., Stefanovich, S.Y. (2002): Synthesis and crystal structure of the new carbonate $NaPb_2(CO_3)_2(OH)$. *Crystallography Reports*, **47**, 217–222.

Béziat, D., Joron, J. L., Monchoux, P., Treuil, M., & Walgenwitz, F. (1991): Geodynamic implications of geochemical data for the Pyrenean ophites (Spain-France). Chemical geology, 89(3-4), 243-262.

Brooker, M.H., Sunder, S., Taylor, P., Lopata, V.J. (1983): Infrared and Raman spectra and X-ray diffraction studies of solid lead(II) carbonates. *Canadian Journal of Chemistry*, **61**, 494–502.

Castillo, M., Torró, L., Campeny, M., Villanova, C., Tauler, E., Melgarejo, J.C. (2009): Mineralogía del Depósito de Uranio Eureka (Castell-estaó, Pirineo, Cataluña). Macla **11**, 53-54.

Foord, E.E. & Mills, B.A. (1978): Biaxiality in 'isometric' and 'dimetric' crystals. *American Mineralogist*, **63**, 316-325.

Hazen, R.M., Hummer, D.R., Hystad G., Downs R.T., J.J. Golden (2016): Carbon mineral ecology: Predicting the undiscovered minerals of carbon. *American Mineralogist*, **101**, 889–906.

Iizuka, Y. (2012): Electron microprobe study of otolith: migratory behaviour and habitat of three major temperature species of eels. JEOL News **47**, 33-50.

Krivovichev, S.V. & Burns, P.C. (2000a): Crystal chemistry of basic lead carbonates. III. Crystal structures of $Pb_3O_2(CO_3)$ and $NaPb_2(OH)(CO_3)_2$. Mineralogical Magazine, **64**, 1077-1087.

Krivovichev, S.V. & Burns, P.C. (2000b): Crystal chemistry of basic lead carbonates. II. Crystal structure of synthetic 'plumbonacrite'. Mineralogical Magazine, **64**, 1069-1075.

Pouchou, J.L. & Pichoir, F. (1988): A simplified version of the "PAP" model for matrix corrections in EPMA. In Microbeam Analysis, Newbury D.E. (Ed.), pp. 319-324. San Francisco Press: San Francisco.

Lane, S.J & Dalton, J.A. (1994): Electron microprobe analysis of geological carbonates. American Mineralogist **79**, 745-749.

Mey, P.H.W., Nagtegaal, P.J.C., Roberti, K.J., & Hartevelt, J.J.A. (1968): Lithostratigraphic subdivision of post-Hercynian deposits in the south-central Pyrenees, Spain. Leidse Geologische Mededelingen, **41**, 221-228.

Muñoz, J. A. (1992): Evolution of a continental collision belt: ECORS-Pyrenees crustal balanced cross-section. In Thrust tectonics (pp. 235-246). Springer Netherlands.

Salvat, F. (2015): PENELOPE-2014: A code system for Monte Carlo simulation of electron and photon transport. OECD/NEA Data Bank, Issy-les-Moulineaux, France.

Siidra, O.I., Jonsson, E., Chukanov, N.V., Pekov, I.V., Zinyakhina, D.O., Polekhovsky, Y.S. & Yapaskurt, V.O. (2015): Grootfonteinite, IMA 2015-051. CNMNC Newsletter, **27**, 1226; Mineralogical Magazine, **79**, 1229–1236.

Spek, A. L. (2009): Structure validation in chemical crystallography. Acta Crystallographica D, 65, 148-155.

Turner, B. R. (1985): Uranium mineralization in the Karoo basin, South Africa. Economic Geology, 80(2), 256-269.

Vergés, J. & Muñoz, J. A. (1990): Thrust sequences in the southern central Pyrenees. Bulletin de la Société géologique de France, **8**, 265-271.

TITLES OF TABLES

447 Table 1. Measured and calculated X-ray powder diffraction data for abellaite.

448 Table 2. Crystallographic data for abellaite.

449 Table 3. Atomic positions for abellaite. The equivalent isotropic thermal displacement
450 parameters correspond to those of the synthetic analogue (Krivovichev & Burns, 2000).

451 Table 4. Raman data for abellaite and for synthetic $NaPb_2(CO_3)_2(OH)$ (Brooker *et al.*,
452 1983).

453 Table 5. FTIR spectroscopy data for abellaite and for synthetic $NaPb_2(CO_3)_2(OH)$ as
454 reported in Brooker *et al.* (1983) and Belokoneva *et al*. (2002).

455 Table 6. Electron microprobe analysis of abellaite.

TABLES

Table 1

I_{obs}	d_{obs} (Å)	I_{calc}	d_{calc} (Å)	*hkl*
3	6.725	2	6.731	002
7	4.550	9	4.555	010
17	4.310	19	4.315	011
2	3.768	2	3.773	012
9	3.362	15	3.366	004
100	3.193	100	3.197	013
3	2.704	1	2.707	014
84	2.627	91	2.630	110
16	2.447	19	2.450	1-2-2,112
6	2.315	6	2.318	015
29	2.275	27	2.278	020
65	2.243	37	2.246	021
		29	2.244	006
<1	2.155	2	2.158	022
19	2.070	22	2.072	1-2-4,114
95	2.029	98	2.031	023
25	2.011	29	2.013	016
1	1.884	4	1.886	024
5	1.770	10	1.772	017
	1.706			numerous
	1.603			numerous
	1.517			numerous
	1.420			numerous
	1.313			numerous
	1.256			numerous
	1.215			numerous

Table 2

Ideal formula	$NaPb_2(CO_3)_2(OH)$
Formula weight	574.41
Crystal system, space group	Hexagonal, $P6_3mc$
Unit-cell dimensions	a = 5.254(2) Å
	c = 13.450(5) Å
V (Å^3)	321.5(2)
Z	2
Density (calculated) (g/cm^3)	5.93

Table 3

Atom	*x*/*a*	*y*/*b*	*z*/*c*	U_{eq}
Na	1/3	-1/3	0.656(5)	0.021
Pb(1)	2/3	1/3	0.821(5)	0.018
Pb(2)	1/3	2/3	0.993(5)	0.019
C(1)	0	0	0.78(1)	0.015
C(2)	0	0	-0.01(1)	0.016
O(1)	0.70(1)	-0.15(1)	0.77(1)	0.020
O(2)	0.25(1)	0.12(1)	0.07(1)	0.025
O(3)	2/3	1/3	0.65(1)	0.046

Table 4

Raman shift (cm^{-1}) This work	Raman shift (cm^{-1}) Brooker *et al*. (1983)	Assignment
202 m	202 m	Lattice modes
280 m, br	285 m, br	
683 m	681 ms	$\upsilon_4 (CO_3^{2-})$
	695 sh	
868 w	868 w	$\upsilon_2 (CO_3^{2-})$
1038 vw	1036 vw	
	1052 w, sh	
1058 vs	1057.2 vs	$\upsilon_1 (CO_3^{2-})$
	1068.4 w	
Most likely overlapped with band at 1391cm^{-1}	~ 1350 w, sh	
1391 s, br	1392 s	$\upsilon_3 (CO_3^{2-})$
	1695 vw	
	1730 vw	Second orders
	1750 vw	
3504 vw, br	3500 vw	OH stretching

Table 5

Infrared (cm^{-1}) This work	Infrared (cm^{-1}) Brooker *et al.* (1983)	Infrared (cm^{-1}) Belokoneva *et al.* (2002)	Assignment
	360 vw		
	455 s	475 m	
	530 w, br		
688 s	693 s	695 s	$\upsilon_4 (CO_3^{2-})$
	825 w		
844 m	843 s	847 s	$\upsilon_2 (CO_3^{2-})$
998 w, br	988 m, br		δ_{PbOH}
1053 w	1053 w	1055 w	$\upsilon_1 (CO_3^{2-})$
1425 vs, br	1435 vs, br	1432 vs, br	$\upsilon_3 (CO_3^{2-})$
1750 w, br	1743 w		Second order
	1758 w		
3500 w, br	3495 w	3480 w, br	OH stretching

Table 6

Element	wt.%	Range	Nominal
Na	3.88	3.69 - 4.03	4.00
K	< DL*		-
Ca	0.29	0.14 - 0.51	-
Pb	72.03	71.14 - 72.7	72.14
C	4.17		4.18
O	19.47		19.50
H	0.17		0.17
Total	100.01		100.00

*Detection limit (DL) for K was in the range 900-1100 ppm

FIGURE CAPTIONS

Figure 1. (a) Location of the Eureka mine in the small town of Castell-estaó, Torre de Capdella (Lleida province), in the Southern Pyrenees. (b) Geological map showing the area around the Eureka mine area (modified from Atlas Geològic de Catalunya 1:5000). (c) Entrance to the gallery where abellaite was found, surrounded by redbed sediments.

Figure 2. (a) Optical photomicrograph of abellaite aggregates. (b) Secondary-electron micrograph showing subhedral abellaite microcrystals. (c) Backscattered electron (BSE) image showing aggregates of idiomorphic, pseudohexagonal abellaite crystals. (d) Detail of the tabular pseudohexagonal crystals, showing prominent pinacoidal faces.

Figure 3. (a) and (b) BSE images showing selected abellaite crystals as well as associated minerals. 1: abellaite...obtained from the probe for chemical analyses. 1: abellaite, 2: vanadinite, 3: Pb-ich intergrowth, 4: Co-rich carbonate, 5: quartz, 6: calcium carbonate, 7: hidrozincite, 8: sphalerite: 9: uraninite, 10: unknown arseniovanadate.

Figure 4. (a) Raman spectrum of abellaite. (b) FTIR transmission spectrum of abellaite. In both figures, the asterisks indicate spectral features that have not been reported in synthetic $NaPb_2(CO_3)_2(OH)$.

FIGURES

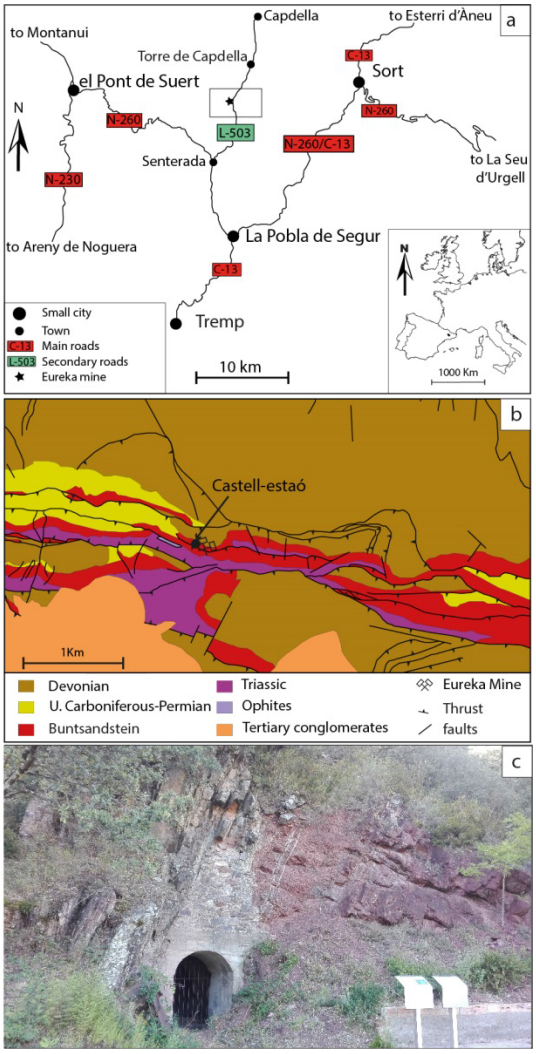

Figure 1

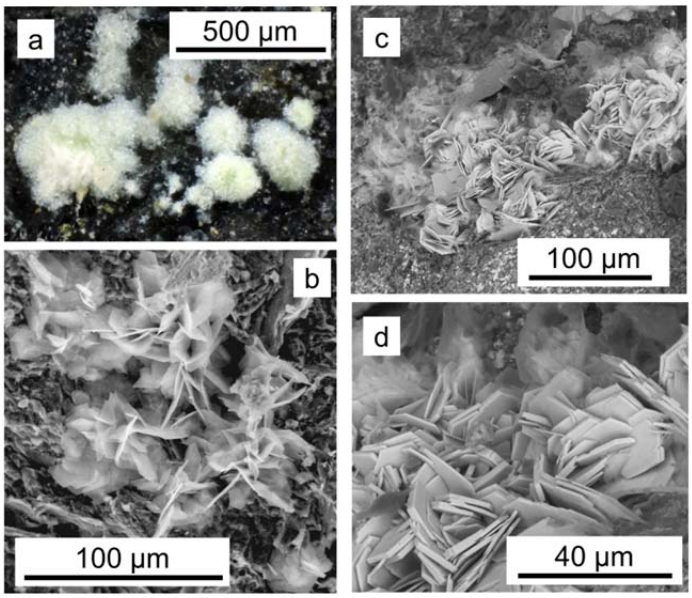

Figure 2

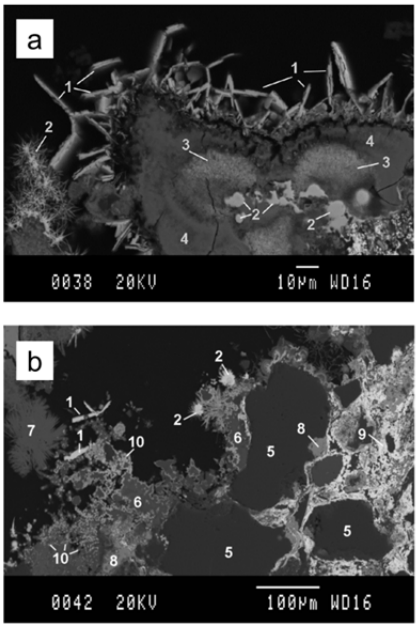
a
1
1
2
3
4
3
2
2
4
0038 20KV 10µm WD16
b
2
1
2
7
1
10
6
8
9
5
6
5
10
8
5
0042 20KV 100µm WD16

Figure 3

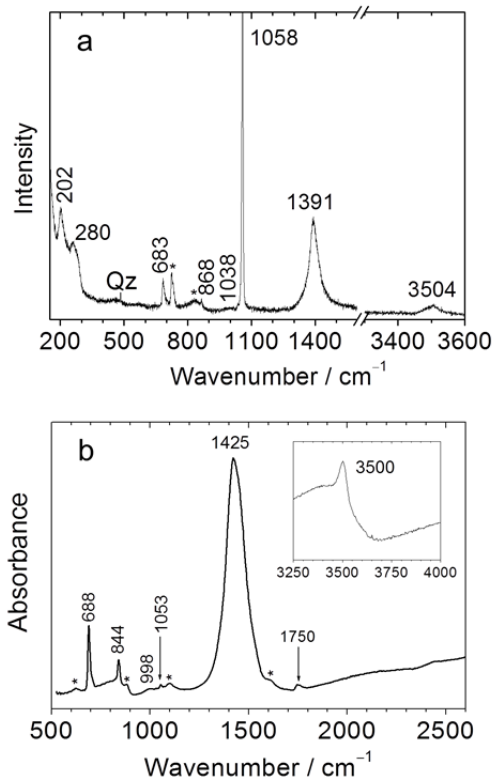
a
1058
Intensity
202
280
Qz
683
868
1038
1391
3504
200 500 800 1100 1400 3400 3600
Wavenumber / cm^{-1}
b
1425
3500
3250 3500 3750 4000
Absorbance
688
844
998
1053
1750
500 1000 1500 2000 2500
Wavenumber / cm^{-1}

Figure 4

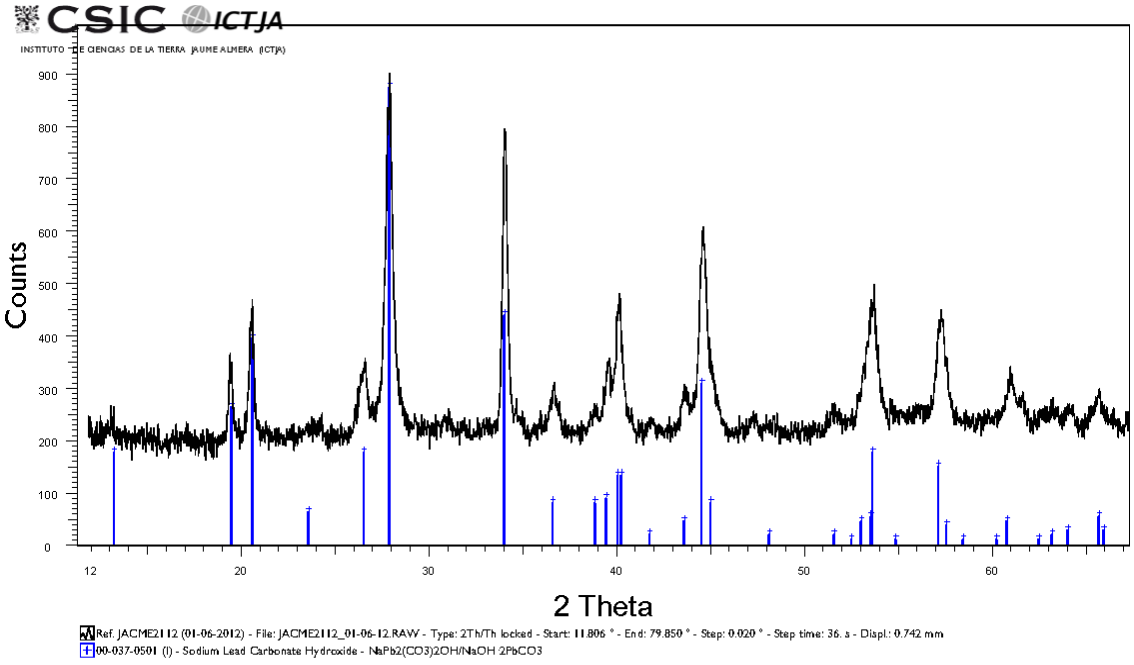

Figure S1. Powder X-ray diffraction scan from dense abellaite aggregates. For comparison, the X-ray diffraction pattern of synthetic $NaPb_2(CO_3)_2(OH)$ from Brooker *et al.* (1983) is also shown.

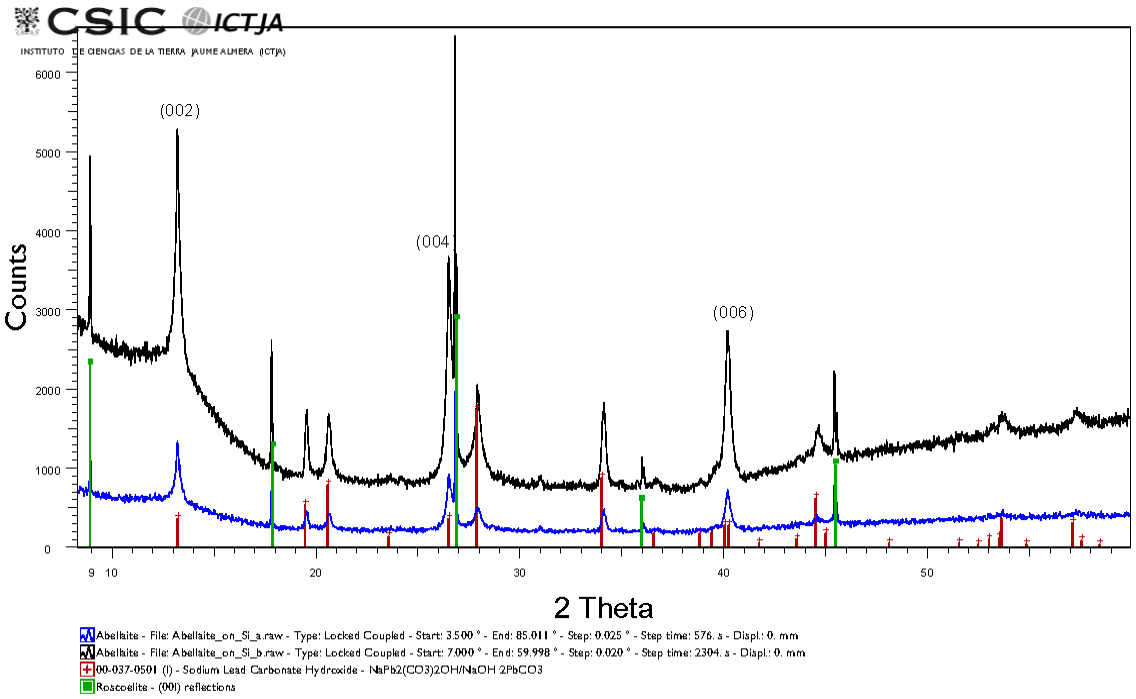

Figure S2. Powder X-ray diffraction scans of abellaite grains on a low-background Si sample holder. For comparison, X-ray diffraction pattern of synthetic $NaPb_2(CO_3)_2(OH)$ from Brooker *et al.* (1983) and roscoelite [only (00*l*) reflections] are included.